Supporting Information for

Environ. Sci. Technol.

Decreases in iron oxide reducibility during microbial reductive dissolution and transformation of ferrihydrite

Meret Aeppli[1,2], Sanja Vranic[1], Ralf Kaegi[2], Ruben Kretzschmar[1], Ashley R. Brown[2] Andreas Voegelin[2], Thomas B. Hofstetter[*,1,2], and Michael Sander[*,1]

[1]Institute of Biogeochemistry and Pollutant Dynamics, ETH Zürich, 8092 Zürich, Switzerland

[2]Swiss Federal Institute of Aquatic Science and Technology (Eawag), 8600 Dübendorf, Switzerland

[*]Corresponding authors:
thomas.hofstetter@eawag.ch
phone +41 58 765 50 76, fax +41 58 765 58 02
michael.sander@env.ethz.ch
phone +41 44 632 83 14, fax +41 44 632 11 22

29 Pages, 22 Figures, 2 Tables

Contents

S1   Chemicals

3-(N-morpholino)propanesulfonic acid (MOPS) was purchased from Sigma. 1,1′- ethylene 2,2′-bipyridyl dibromide (diquat, 99.5 %), 2,2′-azino-bis(3-ethylbenzothiazoline-6-sulfonic acid (ABTS, ≥98%), acetic acid, ammonium fluoride, and iron(III) nitrate nonahydrate were purchased from Sigma-Aldrich. 1,10-phenanthroline hydrochloride monohydrate, 2-(N-morpholino)-ethanesulfonic acid (MES), hydrochloric acid, piperazine-1,4-bis(2-ethanesulfonic acid) (PIPES), and ammonium acetate were purchased from Merck. Hydroxylamine hydrochloride was purchased from Fluka.

S2   Ferrihydrite synthesis

Six-line ferrihydrite was synthesized as described in Schwertmann and Cornell[1]. In brief, 6 g Fe(NO_3)$_3$·9H_2O were added to 0.6 L of 75℃ warm doubly deionized water. The resulting suspension was shaken vigorously before being placed in an oven at 75℃ for 10 min. The suspension was then rapidly cooled on ice and dialyzed for 5 d to remove electrolytes (SpectraPor 7, 10 kD MWCO). Ferrihydrite was used in the incubation experiments within one week of synthesis.

S3   Preparation of bacterial cultures

Shewanella oneidensis strain MR-1 was grown anaerobically at 30℃ in a pre-sterilized, liquid minimal medium (pH 7.4) described by Myers and Nealson[2]. The medium contained 9.0 mM (NH_4)$_2$SO$_4$; 5.7 mM K_2HPO$_4$; 3.3 mM KH_2PO_4; 2.2 mM NaHCO$_3$; 1 mM $MgSO_4$·7H_2O; 0.49 mM $CaCl_2$·2H_2O; 67.2 μM Na$_2$EDTA; 56.6 μM H_3BO_3; 10 μM NaCl; 5.4 μM $FeSO_4$·7H_2O; 5 μM $CoCl_2$·6H_2O; 5 μM $NiCl_2$·6H_2O; 3.9 μM Na$_2$MoO$_4$·2H_2O; 1.5 μM Na$_2$SeO$_4$; 1.3 μM MnCO$_3$; 1 μM $ZnCl_2$; 0.2 μM $CuSO_4$·5H_2O; 20 mg L^{-1} L-arginine HCl; 20 mg L^{-1} L-glutamate; 20 mg L^{-1} L-serine; 100 mM sodium DL-lactate as carbon source and electron donor; and 20 mM fumarate as electron acceptor. Cells were harvested at late-log to early stationary phase and were washed by sequential centrifugation (20 min at 5000 G), removal of the supernatant and resuspension of the resulting pellet in anoxic buffer (pH 7.0, 0.03 M MOPS with 0.01 M NaCl). Anoxic conditions were maintained during the removal of supernatant and resuspension of the pellet by sparging the suspensions with ultrahigh purity N$_2$ (99.999%) through sterile filters (0.22 μm polyethersulfone syringe filters, TPP). The washing step was repeated three times before the washed cell suspension was diluted by addition of anoxic buffer solution (see above) to a cell concentration of ≈10^{10} cells mL^{-1} (corresponds to an optical density of 4 at 600 nm (CARY 100 Bio UV-visible Spectrophotometer), as determined in a cell count by plating).
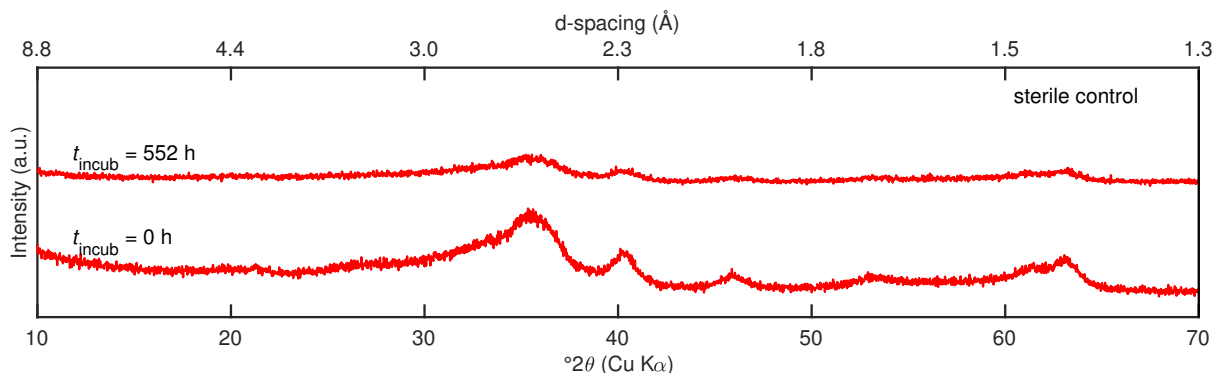
S4 Sterile control experiment

Figure S1 X-ray diffractograms obtained on sample aliquots that were collected at the beginning (t_{incub}=0 h) and at the end (t_{incub}=552 h) of an exemplary sterile control experiment (ferrihydrite, no *S. oneidensis*, pH 7.0 with bicarbonate buffer). No mineral transformation was observed over the duration of the sterile control experiment.
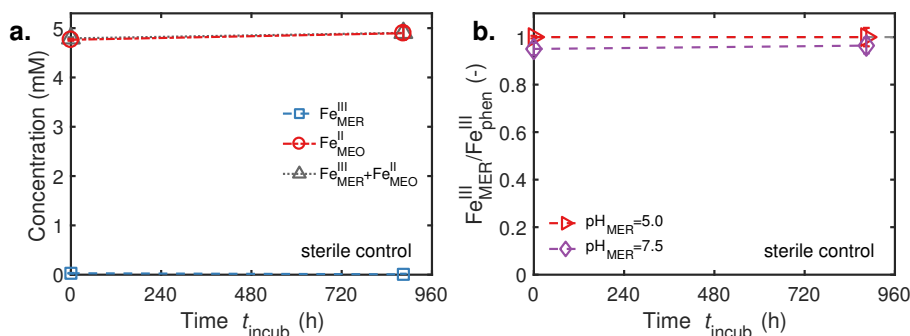

Figure S2 Analyses of iron redox state and iron oxide reducibility at the beginning (t_{incub}=0 h) and at the end (t_{incub}= 884 h) of an exemplary sterile control experiment (ferrihydrite, no *S. oneidensis*, pH 7.0 with PIPES buffer). **a.** Concentrations of Fe^{III} and Fe^{II} were determined using mediated electrochemical reduction (MER) and oxidation (MEO), respectively, as described in the main manuscript. No changes in iron redox state were detected over the duration of the experiment. **b.** Iron oxide reducibility is shown in terms of reduction extents which are presented as fractions of total oxide-Fe^{III} reducible in MER ($Fe^{III}_{MER}/Fe^{III}_{phen}$). Total Fe^{III} ($= Fe^{III}_{phen}$) was determined using the phenanthroline assay (phen). MER measurements were performed at pH_{MER}=5.0 (red triangles) and 7.5 (purple diamonds), both at applied reduction potentials of $E^{MER}_H = -0.35$ V. No changes in iron oxide reducibility were detected over the duration of the sterile control experiment.

S5 Effect of buffer species on microbial reductive dissolution and transformation of ferrihydrite

Previous studies demonstrated that buffer species can affect on the microbial reductive dissolution and transformation of ferrihydrite[3,4] and hence presumably also on the decrease in iron oxide reducibility associated with this transformation. We tested for such effects by performing experiments also with bicarbonate (at initial donor-to-acceptor ratios of 1:16, 1:4 and 1:1) and PIPES (at initial donor-to-acceptor ratios of 1:1, 4:1 and 16:1) buffers in addition to the experiments with MOPS buffer which we discuss in the main manuscript. Microbial Fe^{III} reduction experiments with bicarbonate and PIPES were performed as described in the Materials and Methods Section with the exception that for experiments with bicarbonate, buffer solutions, incubation vials, as well as iron oxide and cell suspensions were purged with a $N_2:CO_2$ (80:20) gas mixture for at least 3 h before transfer into an anoxic glovebox. Over the course of the experiments with bicarbonate and PIPES, we followed microbial Fe^{III} reduction, changes in iron oxide mineralogy, and decreases in iron oxide reducibility as described for the MOPS incubations in the main manuscript. The results of these analyses are shown in Sections S5.1-S5.4.

In general, the rates and extents of microbial Fe^{III} reduction in incubations with bicarbonate and PIPES buffers were similar to those in incubations with MOPS buffer (Figures S3, S4 and 1a-c). The reducibilities of the iron oxides that formed at different initial donor-to-acceptor ratios differed slightly between the three sets of incubations run with the different buffers, reflecting differences in the mineralogical properties of the formed iron oxides, as discussed in the following.

At an initial donor-to-acceptor ratio of 1:16, ferrihydrite transformed exclusively into goethite, both in incubations with bicarbonate and MOPS (Figures S5a, 1d). However, the goethite that formed in the presence of bicarbonate was more reducible than the goethite that formed in the presence of MOPS (Figures S9a, 3d). We attribute the higher reducibility of the former goethite to its smaller particle size (Figures S11a, 1g and S20c; crystallite sizes estimated from X-ray diffractograms were 6.9±0.3 and 13.1±0.2 nm, respectively).

At an initial donor-to-acceptor ratio of 1:4, ferrihydrite transformed predominantly into goethite and only little magnetite formed, both in incubations with bicarbonate and MOPS (Figure S5b, S16a). The overall reducibility of the final iron oxide mixture was higher for incubations with bicarbonate than MOPS buffer (Figures S9b, S18a), in good agreement with the smaller particle size of the goethite that formed in the presence of bicarbonate than the goethite that formed in the presence of MOPS (Figures S11b, S17a; crystallite sizes estimated from X-ray diffractograms: 3.6±0.1 and 6.6±0.5 nm, respectively).

At an initial donor-to-acceptor ratio of 1:1, ferrihydrite transformed into goethite-magnetite mixtures irrespective of which buffer was used. However, the composition of the formed mixtures varied between incubations with different buffers: In incubations with bicarbonate, the transformation of ferrihydrite into magnetite with goethite as an intermediate phase was more pronounced (Figure S5c) than in incubations with PIPES (Figure S7a) and MOPS (Figure

1e). The iron oxide mixture that formed in the presence of MOPS was less reducible (Figure 3e) than the iron oxide mixtures that formed in the presence of bicarbonate (Figure S9c) and PIPES (Figure S10a). We attribute the low reducibility of the former to the larger particle size of the magnetite that formed in the presence of MOPS (Figures 1h and S20f; crystallite size from X-ray diffractograms: 176.6±3.3 nm) as compared to the magnetite that formed in the presence of bicarbonate and PIPES (Figures S11c and S11d, respectively; crystallite sizes from X-ray diffractograms: 36.0±5.2 and 75.1±5.0 nm, respectively).

At an initial donor-to-acceptor ratio of 4:1, ferrihydrite transformed into goethite-magnetite mixtures with almost identical composition in both incubations with PIPES and MOPS (Figures S7b and S16b). The formed iron oxide mixtures had similar reducibilities (Figures S10b and S18b), and the formed particles were of similar size (Figures S11e and S17b; crystallite sizes from X-ray diffractograms: 52.3±1.0 nm for magnetite and 3.2±0.4 nm for goethite in the PIPES incubations, and 58.7±0.9 nm for magnetite and 3.0±0.2 nm for goethite in the MOPS incubations).

At an initial donor-to-acceptor ratio of 16:1, ferrihydrite transformation was incomplete in both PIPES and MOPS incubations but proceeded to a larger extent in the MOPS incubations (Figures S10c and 1f). The final iron oxide mixtures in the two incubations with PIPES and MOPS showed similar reducibilities (Figures S10c and 3f) and particle morphologies (Figures S11f, 1i and S20i).
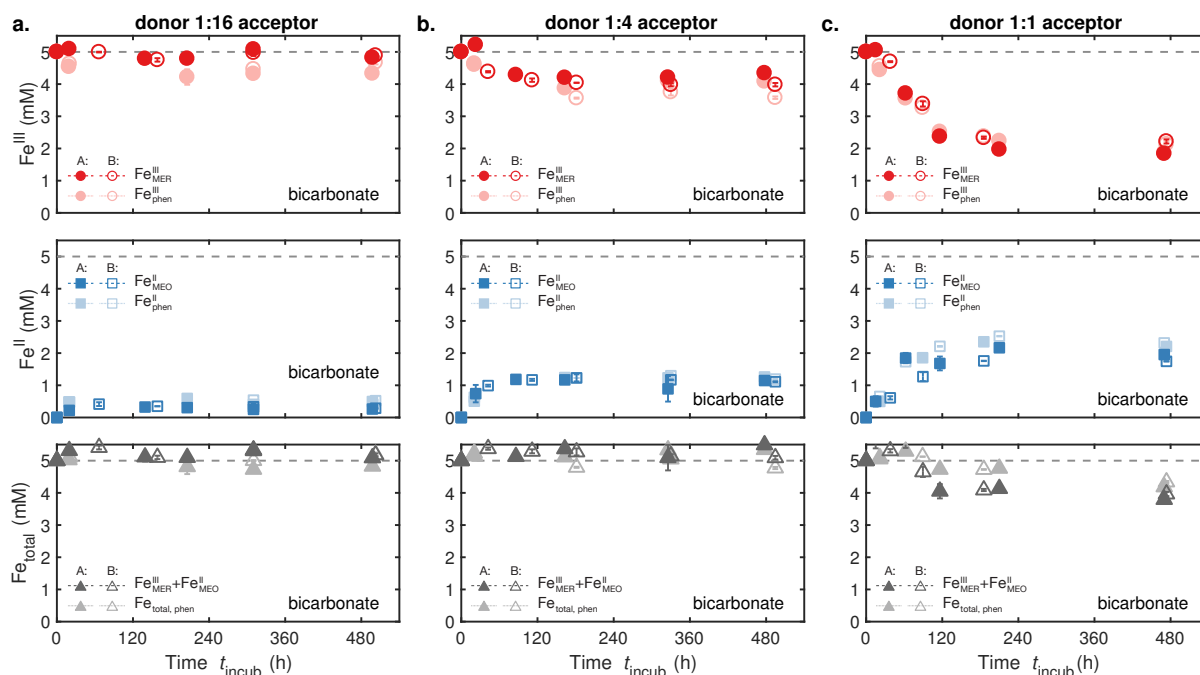
S5.1 Microbial Fe^{III} reduction

Figure S3 Microbial Fe^{III} reduction in incubations buffered to pH 7.0 using bicarbonate at initial donor-to-acceptor ratios of 1:16 (panel **a.**), 1:4 (panel **b.**) and 1:1 (panel **c.**). Data are shown for duplicate incubation vials (A and B in filled and open symbols, respectively). Concentrations of Fe^{III} reduced in mediated electrochemical reduction (Fe$^{III}_{MER}$) and Fe^{II} oxidized in mediated electrochemical oxidation (Fe$^{II}_{MEO}$) during the incubations were determined from the current responses in MER and MEO, respectively, as described in the main manuscript. The sums of Fe$^{III}_{MER}$ and Fe$^{II}_{MEO}$ are shown as grey triangles. Concentrations of Fe$^{II}_{phen}$ and Fe$_{total, phen}$ were determined using the phenanthroline assay (phen). Fe$^{III}_{phen}$ was calculated by subtracting Fe$^{II}_{phen}$ from Fe$_{total, phen}$.
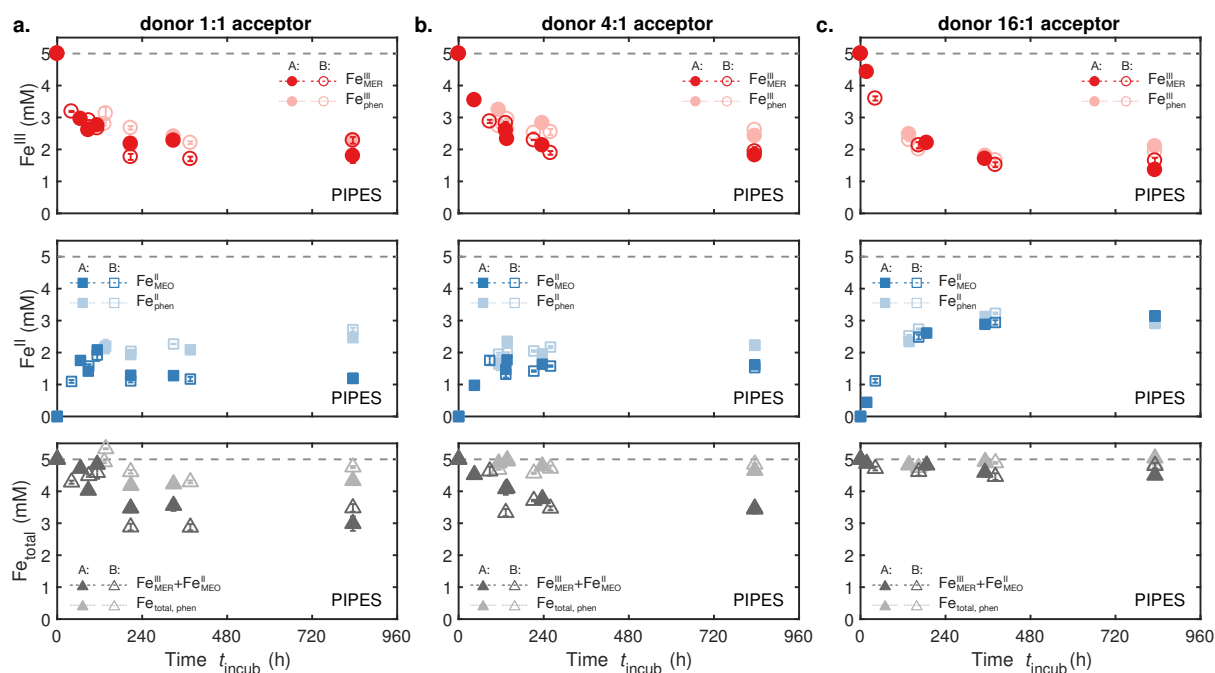
Figure S4 Microbial Fe^{III} reduction in incubations buffered to pH 7.0 using PIPES at initial donor-to-acceptor ratios of 1:1 (panel **a.**), 4:1 (panel **b.**) and 16:1 (panel **c.**). Data are shown for duplicate incubation vials (A and B in filled and open symbols, respectively). Concentrations of Fe^{III} reduced in mediated electrochemical reduction (Fe^{III}_{MER}) and Fe^{II} oxidized in mediated electrochemical oxidation (Fe^{II}_{MEO}) during the incubations were determined from the current responses in MER and MEO, respectively, as described in the main manuscript. The sums of Fe^{III}_{MER} and Fe^{II}_{MEO} are shown as grey triangles. Concentrations of Fe^{II}_{phen} and $Fe_{total, phen}$ were determined using the phenanthroline assay (phen). Fe^{III}_{phen} was calculated by subtracting Fe^{II}_{phen} from $Fe_{total, phen}$.

S5.2   Iron oxide transformations during microbial Fe$^{\text{III}}$ reduction

Figure S5 Changes in iron oxide mineralogy during incubations at initial donor-to-acceptor ratios of 1:16 (panel **a.**), 1:4 (panel **b.**), and 1:1 (panel **c.**), all buffered to pH 7.0 using bicarbonate. Data are shown for duplicate incubation vials (A and B in filled and open symbols, respectively). Molar Fe$^{\text{III}}$ fractions in ferrihydrite (green circles), goethite (orange triangles), and magnetite (black squares) were determined by X-ray diffraction analysis as described in Aeppli et al.[5]. The mass fractions of crystalline lepidocrocite were <0.4% in all samples. The mass fractions of crystalline siderite were <0.6% in samples collected during incubations at initial donor-to-acceptor ratios of 1:16 and 1:4. In the incubation at initial donor-to-acceptor ratio of 1:1, final mass fractions of crystalline siderite of 12% and 4.7% formed in incubation vials A and B, respectively (not shown because siderite is a Fe$^{\text{II}}$ oxide).
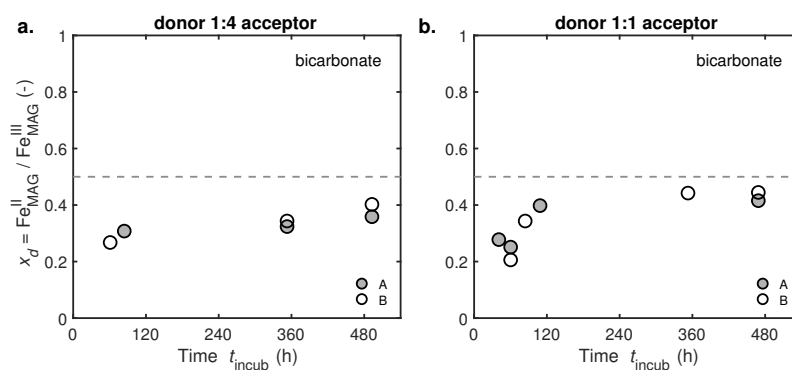
Figure S6 Changes in magnetite stoichiometry, $x_d = \text{Fe}^{\text{II}}_{\text{MAG}}/\text{Fe}^{\text{III}}_{\text{MAG}}$, during incubations at initial donor-to-acceptor ratios of 1:4 (panel **a.**), and 1:1 (panel **b.**), both buffered to pH 7.0 using bicarbonate. Data are shown for duplicate incubation vials (A and B in filled and open symbols, respectively). Magnetite stoichiometries were determined using eq. S1 in Section S13. Note that no magnetite formed in the experiment at initial donor-to-acceptor ratio of 1:16.
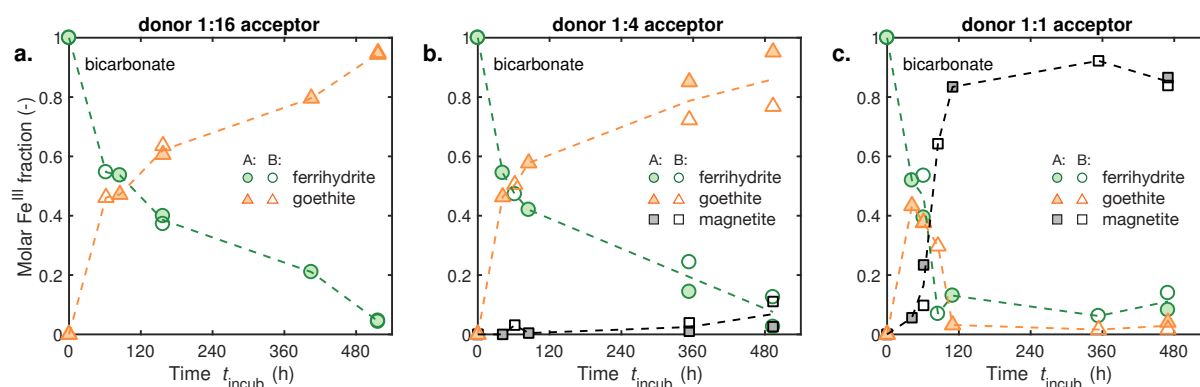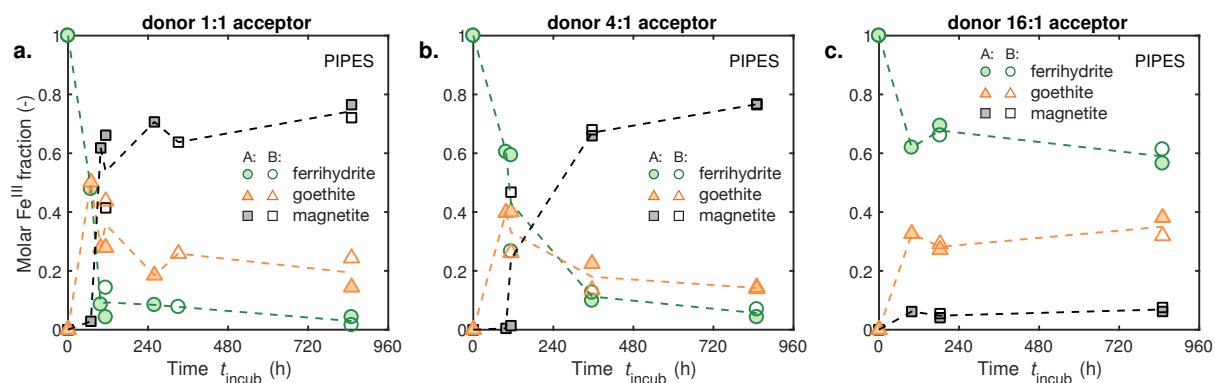
Figure S7 Changes in iron oxide mineralogy during incubations at initial donor-to-acceptor ratios of 1:1 (panel **a.**), 4:1 (panel **b.**), and 16:1 (panel **c.**), all buffered to pH 7.0 using PIPES. Data are shown for duplicate incubation vials (A and B in filled and open symbols, respectively). Molar Fe^{III} fractions in ferrihydrite (green circles), goethite (orange triangles) and magnetite (black squares) were determined by X-ray diffraction analysis as described in Aeppli et al. [5]. The mass fractions of crystalline siderite and lepidocrocite were <2.9% in all samples.
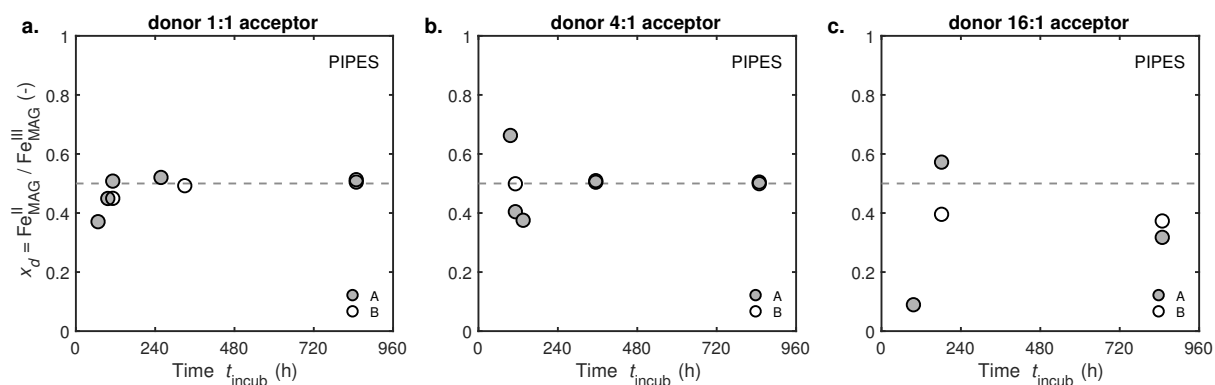
Figure S8 Changes in magnetite stoichiometry, $x_d = Fe^{II}_{MAG}/Fe^{III}_{MAG}$, during incubations at initial donor-to-acceptor ratios of 1:1 (panel **a.**), 4:1 (panel **b.**), and 16:1 (panel **c.**), all buffered to pH 7.0 using PIPES. Data are shown for duplicate incubation vials (A and B in filled and open symbols, respectively). Magnetite stoichiometries were determined using eq. S1 in Section S13.

S5.3   Decreases in iron oxide reducibility during microbial Fe^{III} reduction

Figure S9 Changes in iron oxide reducibility during microbial iron oxide reduction as assessed using mediated electrochemical reduction (MER). Incubations were performed at initial donor-to-acceptor ratios of 1:16 (panel **a.**), 1:4 (panel **b.**) and 1:1 (panel **c.**), all buffered to pH 7.0 using bicarbonate. MER data are shown for duplicate incubation vials (A and B in filled and open symbols, respectively). Changes in the extents of oxide-Fe^{III} reduction over the course of the incubations are shown. Reduction extents are presented as the fraction of total oxide-Fe^{III} reducible in MER (Fe$_{MER}^{III}$/Fe$_{phen}^{III}$). Fe$_{phen}^{III}$ was determined using the phenanthroline assay (phen). MER measurements were performed at pH$_{MER}$=5.0 (red triangles) and 7.5 (purple diamonds), both at applied reduction potentials of $E_H^{MER} = -0.35$ V.
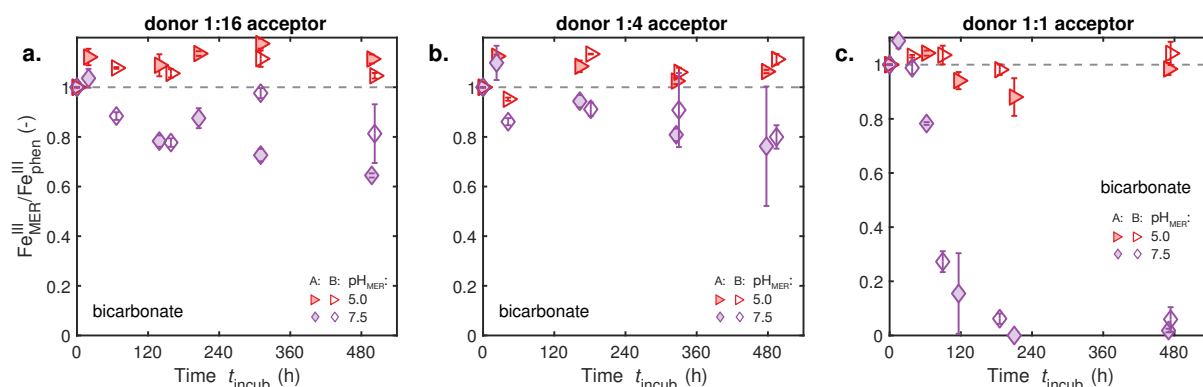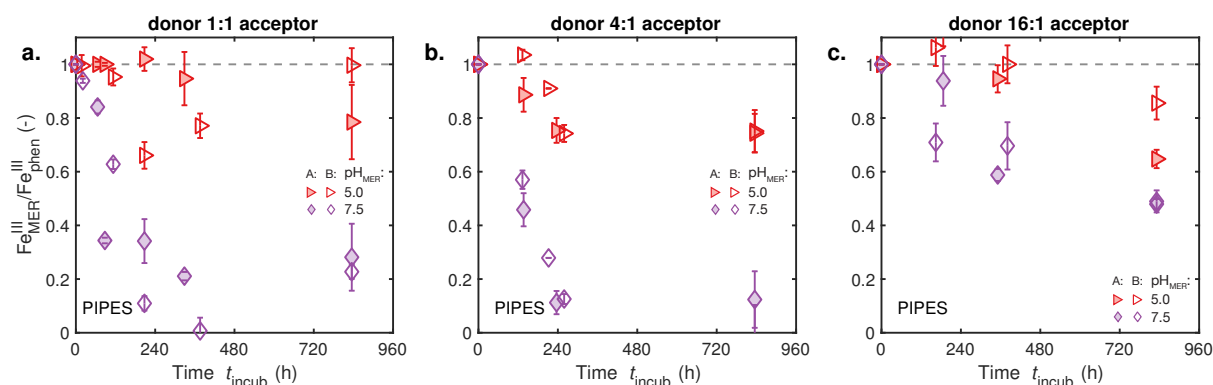

Figure S10 Changes in iron oxide reducibility during microbial iron oxide reduction as assessed using mediated electrochemical reduction (MER). Incubations were performed at initial donor-to-acceptor ratios of 1:1 (panel **a.**), 4:1 (panel **b.**) and 16:1 (panel **c.**), all buffered to pH 7.0 using PIPES. MER data are shown for duplicate incubation vials (A and B in filled and open symbols, respectively). Changes in the extents of oxide-Fe^{III} reduction over the course of the incubations are shown. Reduction extents are presented as the fraction of total oxide-Fe^{III} reducible in MER (Fe$_{MER}^{III}$/Fe$_{phen}^{III}$). Fe$_{phen}^{III}$ was determined using the phenanthroline assay (phen). MER measurements were performed at pH$_{MER}$=5.0 (red triangles) and 7.5 (purple diamonds), both at applied reduction potentials of $E_H^{MER} = -0.35$ V.

S5.4 Electron microscopy images of iron oxides

Figure S11 Selected electron microscopy images of iron oxides collected during incubations buffered to pH 7.0 using bicarbonate (**a.-c.**) and PIPES (**e.-g.**). The initial donor-to-acceptor ratio of the respective experiment and the time of iron oxide suspension collection, t_{incub}, are reported on the plots. Images were recorded using a secondary electron detector.

S6   X-ray Diffraction Analysis

S6.1   Sample preparation and analysis

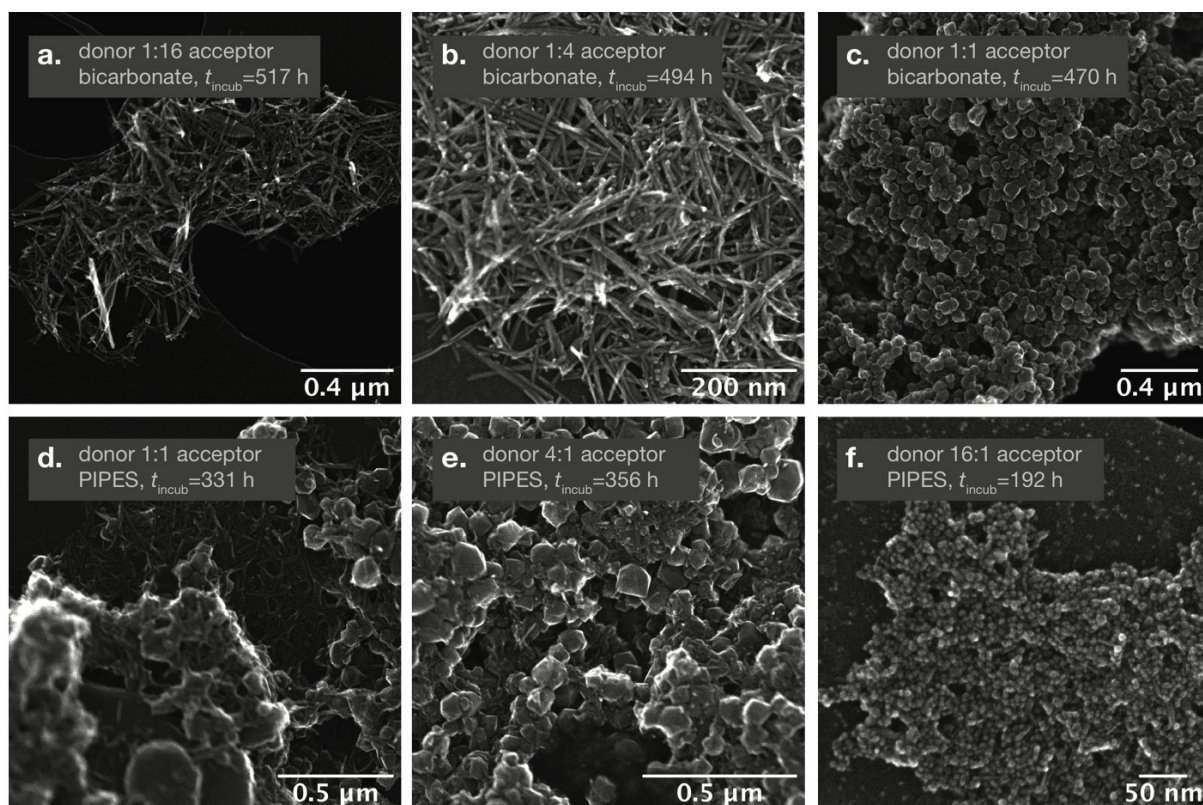We determined changes in iron oxide mineralogy in the 7.0 mL aliquots collected over the course of the incubations using X-ray diffraction analysis as described in Aeppli et al.[5]. In brief, 4.5 mL of the 7.0 mL aliquots (see above) were washed, re-suspended in pure ethanol and deposited onto zero background wafers (510 orientation, Sil'tronix). After drying, the slides were inserted into anoxic sample holders and taken out of the glovebox. X-ray diffractograms were then recorded on a D8 Advance instrument (Bruker) from 10 to 70°2θ (step size 0.02°2θ and 6 or 10 s acquisition time per step) in Bragg-Brentano geometry using Cu Kα radiation (λ =1.5418 Å, 40 kV and 40 mA) and a high-resolution energy-dispersive 1-D detector (LYNXEYE).

We determined the mass fractions of ferrihydrite, goethite, magnetite, siderite and lepidocrocite in each aliquot by Rietveld quantitative phase analysis in TOPAS (Version 5) of the Bruker DIFFRAC.SUITE software package. For Rietveld analysis, we used published structure files for goethite, magnetite, siderite and lepidocrocite (Inorganic Crystal Structure Database, FIZ Karlsruhe) and calibrated ferrihydrite as hkl-phase using the partial or no known crystal structure method (PONKCS)[6], as described in our previous publications[5,7]. In Rietveld analysis, we only included iron oxides that showed characteristic diffraction peaks in the collected X-ray diffractograms. Preferred orientation of goethite (100, 110) and lepidocrocite (010) was considered in Rietveld analysis (March Dollase method, TOPAS). Crystallite sizes of goethite and magnetite were calculated from the integral breath (i.e., peak area divided by peak height) of characteristic diffraction peaks of the respective oxide.

S6.2 X-ray Diffractograms

Figure S12 Selected X-ray diffractograms obtained during incubations buffered to pH 7.0 using MOPS at initial donor-to-acceptor ratios of 1:16 (**a.**) and 1:4 (**b.**). Sample aliquots were collected from duplicate incubation vials A (red) and B (blue) at selected time points, t_{incub}, during the experiments as indicated on the plots. Goethite and magnetite diffraction peaks are labelled with G and M, respectively.
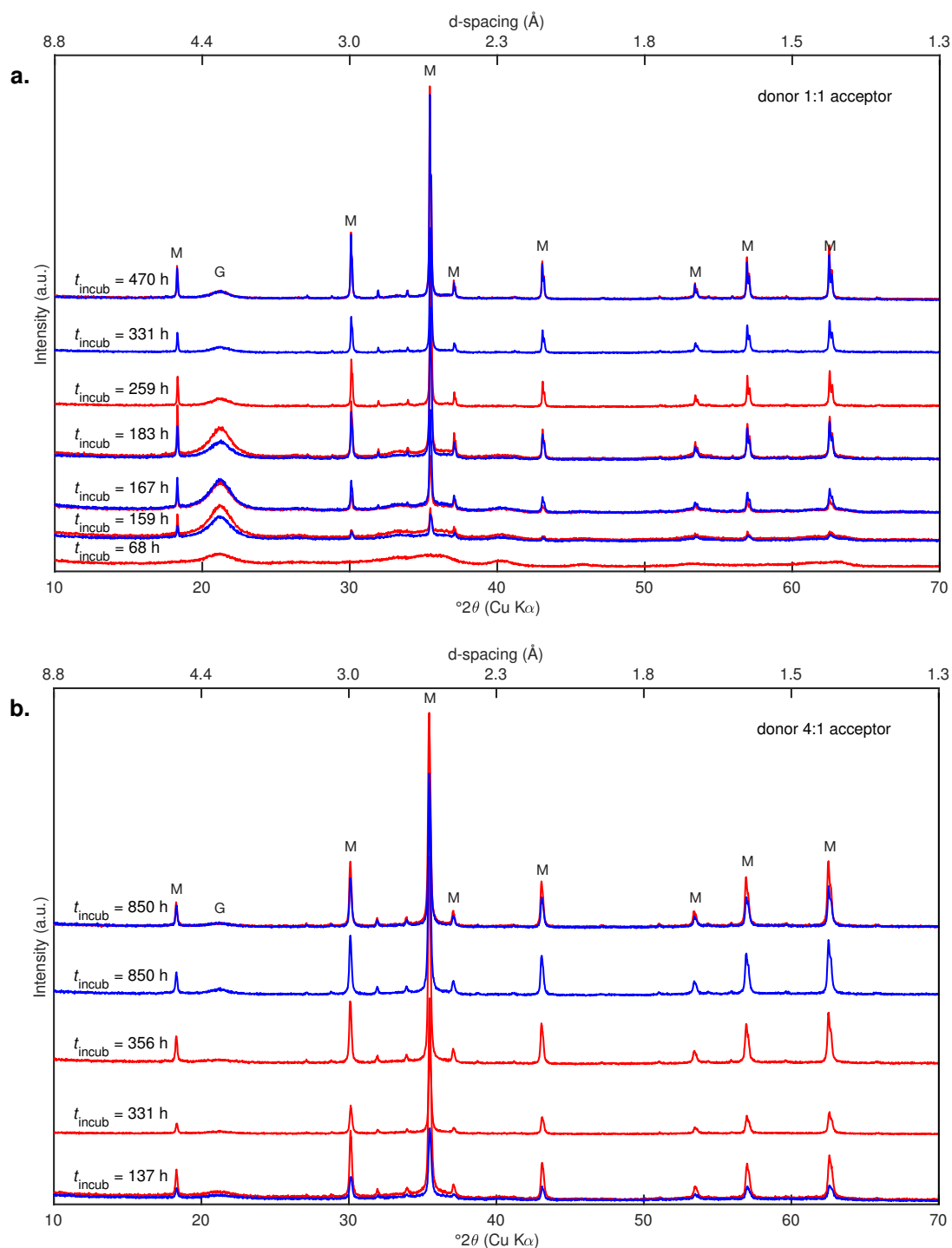
Figure S13 Selected X-ray diffractograms obtained during incubations buffered to pH 7.0 using MOPS at initial donor-to-acceptor ratios of 1:1 (**a.**) and 4:1 (**b.**). Sample aliquots were collected from duplicate incubation vials A (red) and B (blue) at selected time points, t_{incub}, during the experiments as indicated on the plots. Goethite and magnetite diffraction peaks are labelled with G and M, respectively.

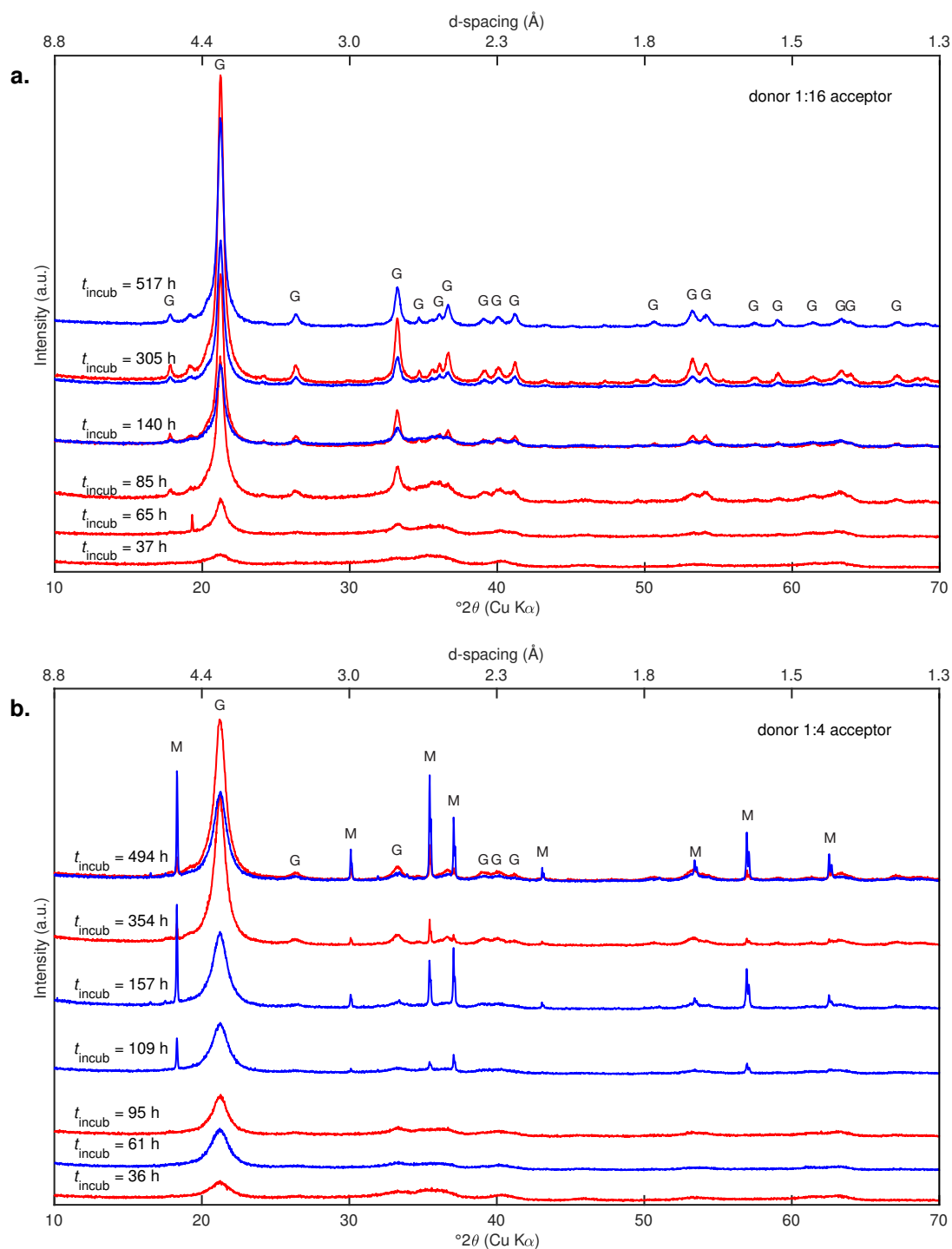**Figure S14** Selected X-ray diffractograms obtained during the incubation buffered to pH 7.0 using MOPS at a initial donor-to-acceptor ratio of 16:1. Sample aliquots were collected from duplicate incubation vials A (red) and B (blue) at selected time points, t_{incub}, during the experiment as indicatedon the plot. Goethite and magnetite diffraction peaks are labelled with G and M, respectively.
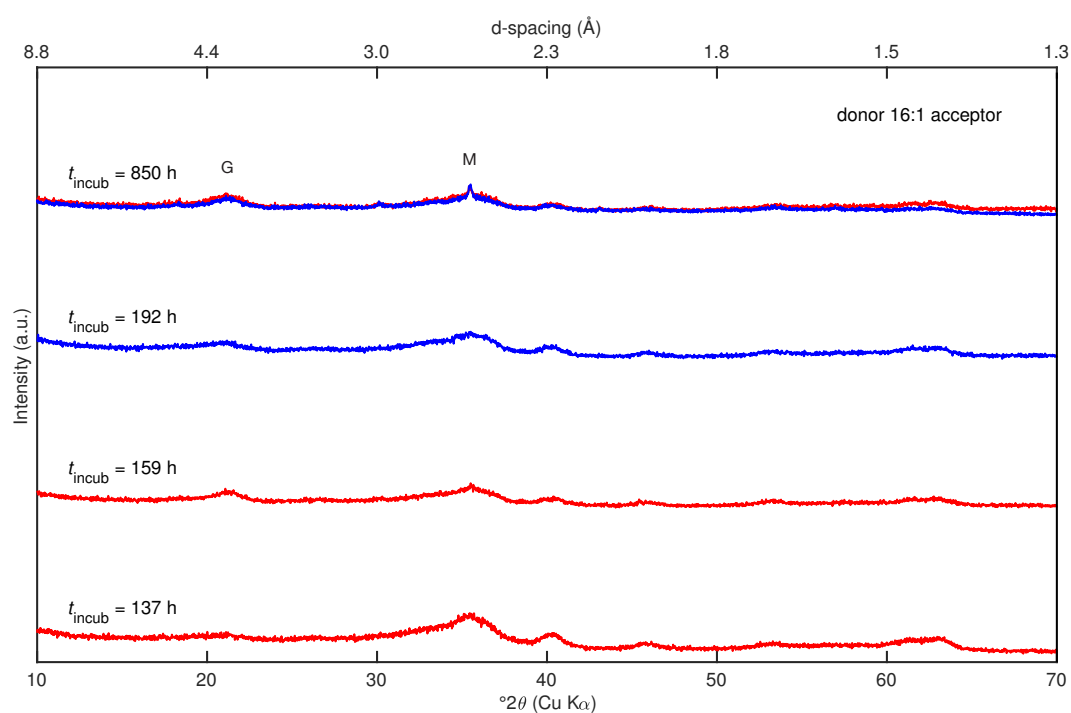
S6.3 Results of Rietveld fitting

Table S1 Mass fractions in weight-% of ferrihydrite (hkl phase), magnetite (MAG), goethite (GOE), siderite (SID) and lepidocrocite (LEP) as determined by Rietveld analysis over the course of incubations buffered to pH 7.0 using MOPS at initial donor-to-acceptor ratios of 1:16, 1:4, and 1:1. The goodness of the fit (GOF) corresponds to R_{wp}/R_{exp}, whereby R_{wp} is the weighted profile R factor and R_{exp} is the expected R factor. All fits were of high quality as GOF < 2, except for the fit labelled with *.

donor-to-acceptor ratio	t_{incub} (h)	Vial	hkl phase (%)	MAG (%)	GOE (%)	SID (%)	LEP (%)	GOF
1:16	0	A	100	0	0	0	0	0.000
1:16	0	B	100	0	0	0	0	0.000
1:16	36.5	A	70	1	29	0	0	1.033
1:16	85	A	63	0	36	0	0	1.312
1:16	140	A	49	1	50	0	0	1.667
1:16	140	B	47	0	53	0	0	1.368
1:16	305	A	16	1	82	1	0	1.857
1:16	305	B	19	1	80	0	0	1.600
1:16	516.5	A	4	1	94	0	0	2.283*
1:16	516.5	B	3	1	96	1	0	1.732
1:4	0	A	100	0	0	0	0	0.000
1:4	0	B	100	0	0	0	0	0.000
1:4	36.5	A	65	0	34	0	0	1.059
1:4	61.75	B	45	0	55	0	0	1.055
1:4	109.5	B	31	6	62	0	0	1.117
1:4	157	B	11	20	68	0	0	1.207
1:4	353.5	A	0	5	95	0	0	1.243
1:4	493.5	A	0	6	94	0	0	1.268
1:4	493.5	B	0	29	70	1	0	1.334
1:1	0	A	100	0	0	0	0	0.000
1:1	0	B	100	0	0	0	0	0.000
1:1	68.5	A	69	0	31	0	0	1.079
1:1	159	A	41	7	51	0	0	1.272
1:1	159	B	39	11	50	0	0	1.192
1:1	167	A	38	15	47	0	0	1.269
1:1	167	B	29	25	46	0	0	1.223
1:1	183	A	15	39	45	1	0	1.409
1:1	183	B	11	49	39	1	0	1.244
1:1	259	A	5	63	31	1	0	1.255
1:1	331	B	6	63	30	1	0	1.245
1:1	850	A	3	67	28	1	0	1.332
1:1	850	B	5	67	26	1	0	1.342

Table S2 Mass fractions in weight-% of ferrihydrite (hkl phase), magnetite (MAG), goethite (GOE), siderite (SID) and lepidocrocite (LEP) as determined by Rietveld analysis over the course of incubations buffered to pH 7.0 using MOPS at initial donor-to-acceptor ratios of 4:1 and 16:1. The goodness of the fit (GOF) corresponds to R_{wp}/R_{exp}, whereby R_{wp} is the weighted profile R factor and R_{exp} is the expected R factor. All fits were of high quality as GOF < 2.

donor-to-acceptor ratio	t_{incub} (h)	Vial	hkl phase (%)	MAG (%)	GOE (%)	SID (%)	LEP (%)	GOF
4:1	0	A	100	0	0	0	0	0.000
4:1	0	B	100	0	0	0	0	0.000
4:1	136.5	A	23	64	13	1	0	1.347
4:1	136.5	B	33	48	19	1	0	1.132
4:1	159	A	15	68	16	1	0	1.191
4:1	331	A	9	78	12	1	0	1.334
4:1	356	B	8	77	14	1	0	1.321
4:1	850	A	10	77	11	1	0	1.359
4:1	850	B	10	75	14	1	0	1.345
16:1	0	A	100	0	0	0	0	0.000
16:1	0	B	100	0	0	0	0	0.000
16:1	68.5	A	75	3	22	0	0	1.078
16:1	192	A	72	3	25	0	0	1.075
16:1	192	B	64	2	34	0	0	1.081
16:1	850	A	54	5	41	0	0	1.088
16:1	850	B	47	10	43	0	0	1.066

S7   Details on electron microscopy investigations

We recorded electron microscopy images of the iron oxides in the suspension aliquots collected over the course of the incubations as described in Aeppli et al.[5]. In brief, 0.5 mL of the 7.0 mL aliquots (see above) were washed, re-suspended in doubly deionized water and drop-deposited onto holey carbon grids. The iron oxide particles on the grids were investigated on a dedicated scanning transmission electron microscope (STEM, 2700Cs, Hitachi) operated at an acceleration voltage of 200 kV. Images were recorded using either a secondary electron or high angular annular dark field detector.

S8   Setup of electrochemical cells

MER and MEO cells consisted of glassy carbon cylinders (9 mL, GAZ 1, HTW) that served as working electrodes and held the reaction solution, which was continuously stirred by Teflon-coated stir bars. We used platinum wires as counter electrodes that were separated from the working electrode compartments by glass frits (PORE E tubes, ACE glass). The reduction potentials applied to the working electrodes of the MER and MEO cells were measured against Ag/AgCl reference electrodes (Re1B, ALS) but are reported herein versus the standard hydrogen electrode.

S9 Matlab code for current peak analysis

Analysis of reductive and oxidative current peaks was performed using the baseline fit function and the bioinformatics toolbox in Matlab (MathWorks), as shown below.

```matlab
% --------------------------------------------------------------------------
% import data
% --------------------------------------------------------------------------
[FName,PathName]=uigetfile('*.txt','Select Text file');
sample=importdata([PathName,FName]);
% number of measurement _xxx
time_xxx=sample.data(:,1);
for i=2:length(time_xxx);
    if time_xxx(i)-time_xxx(i-1)==10;
        time_xxx(i)=time_xxx(i)-5;
    else
        time_xxx(i)=time_xxx(i);
    end
end
Dat_xxx=sample.data(:,2:9);
%%
% --------------------------------------------------------------------------
% Transform MEO data
% --------------------------------------------------------------------------
Dat_imp(:,7)=Dat_imp(:,7)*-1;
Dat_imp(:,8)=Dat_imp(:,8)*-1;
% --------------------------------------------------------------------------
% baseline subtraction
% --------------------------------------------------------------------------
[Dat_xxx(:,1),bs(:,1)] = bf(Dat_xxx(:,1),'confirm',16);
[Dat_xxx(:,2),bs(:,2)] = bf(Dat_xxx(:,2),'confirm',16);
[Dat_xxx(:,3),bs(:,3)] = bf(Dat_xxx(:,3),'confirm',16);
[Dat_xxx(:,4),bs(:,4)] = bf(Dat_xxx(:,4),'confirm',16);
[Dat_xxx(:,5),bs(:,5)] = bf(Dat_xxx(:,5),'confirm',16);
[Dat_xxx(:,6),bs(:,6)] = bf(Dat_xxx(:,6),'confirm',16);
[Dat_xxx(:,7),bs(:,7)] = bf(Dat_xxx(:,7),'confirm',16);
[Dat_xxx(:,8),bs(:,8)] = bf(Dat_xxx(:,8),'confirm',16);
% --------------------------------------------------------------------------
% save baseline subtraction
% --------------------------------------------------------------------------
csvwrite('bs_xxx.csv',Dat_xxx)
% --------------------------------------------------------------------------
% manually select start and end points of peaks and save
% as c1, c2 etc.
% --------------------------------------------------------------------------
msviewer(time_xxx,Dat_xxx(:,1))
% --------------------------------------------------------------------------
% User Input Section
% --------------------------------------------------------------------------
```

```matlab
45  NPeaks=[3,3,3,3,3,3,3,3]; % _xxx
46  sep=[c1,c2,c3,c4,c5,c6,c7,c8];
47  sep_start=sep([1:2:5],:); % select all peak start points
48  sep_start=round(sep_start./5)*5/5; % round to 5 (as dt=5)
49  sep_end=sep([2:2:6],:); % select all peak end points
50  sep_end=round(sep_end./5)*5/5; % round to 5 (as dt=5)
51  % -------------------------------------------------------------------------
52  % Parameters and matrices
53  % -------------------------------------------------------------------------
54  f=96485.3365;
55  dt=5;
56  Out=zeros(sum(NPeaks),2);
57  % -------------------------------------------------------------------------
58  % Loop over currents and peaks
59  % -------------------------------------------------------------------------
60  for i=1:length(Dat_xxx(1,:)) % for currents 1 to 8
61
62      for j=1:NPeaks(i) % for all peaks
63          i1=sep_start(j,i);
64          i2=sep_end(j,i);
65          sI=Dat_xxx(i1:i2,i);
66
67          % Peak maximum
68          clear ind_imax
69          [¬,ind_imax]=max(sI);
70          clear imax
71          imax=max(sI);
72          Out(sum(NPeaks(1:(i-1)))+j,1)=imax;
73
74          % Integration
75          clear int
76          int=zeros(1,length(sI));
77          int(1)=0;
78          for k=2:length(sI)
79              int(k)=int(k-1)+((sI(k)+sI(k-1))/2)*dt;
80          end
81          int=int/f;
82          Out(sum(NPeaks(1:(i-1)))+j,2)=int(end);
83  % -------------------------------------------------------------------------
84  % Prepare Output
85  % -------------------------------------------------------------------------
86          RawDatOut_xxx(sum(NPeaks(1:(i-1)))+j,1:i2-i1+1)=[sI];
87      end
88  end
89  % -------------------------------------------------------------------------
90  % Write Output
91  % -------------------------------------------------------------------------
92  RawDatOut_xxx(sum(NPeaks(1:(i-1)))+j+1,1:length(time_xxx))=[time_xxx];
93  csvwrite('Output_xxx.csv',Out)
```

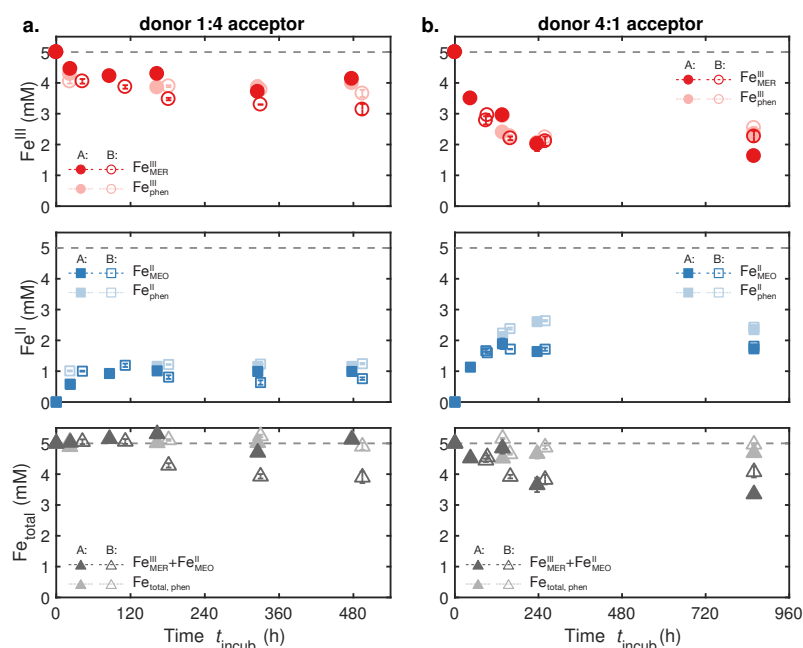# S10 Incubations at intermediate initial donor-to-acceptor ratios

Figure S15 Microbial Fe^{III} reduction in incubations buffered to pH 7.0 using MOPS at initial donor-to-acceptor ratios of 1:4 (panel **a.**) and 4:1 (panel **b.**). Data are shown for duplicate incubation vials (A and B in filled and open symbols, respectively). Concentrations of Fe^{III} reduced in mediated electrochemical reduction (Fe^{III}_{MER}) and Fe^{II} oxidized in mediated electrochemical oxidation (Fe^{II}_{MEO}) during the incubations were determined from the current responses in MER and MEO, respectively, as described in the main manuscript. The sums of Fe^{III}_{MER} and Fe^{II}_{MEO} are shown as grey triangles. Concentrations of Fe^{II}_{phen} and $Fe_{total, phen}$ were determined using the phenanthroline assay (phen). Fe^{III}_{phen} was calculated by subtracting Fe^{II}_{phen} from $Fe_{total, phen}$.
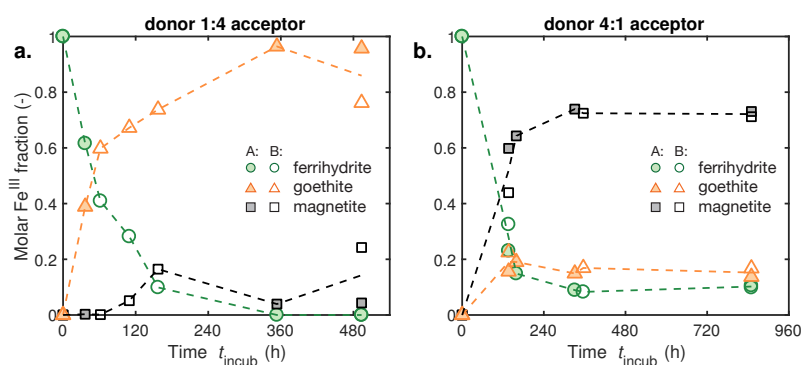

Figure S16 Changes in iron oxide mineralogy during incubations buffered to pH 7.0 using MOPS at initial donor-to-acceptor ratios of 1:4 (panel **a.**) and 4:1 (panel **b.**). Data are shown for duplicate incubation vials (A and B in filled and open symbols, respectively). Molar Fe^{III} fractions in ferrihydrite (green circles), goethite (orange triangles) and magnetite (black squares) were determined by X-ray diffraction analysis as described in Aeppli et al.[5]. The mass fractions of crystalline siderite and lepidocrocite were <1.3% in all samples.
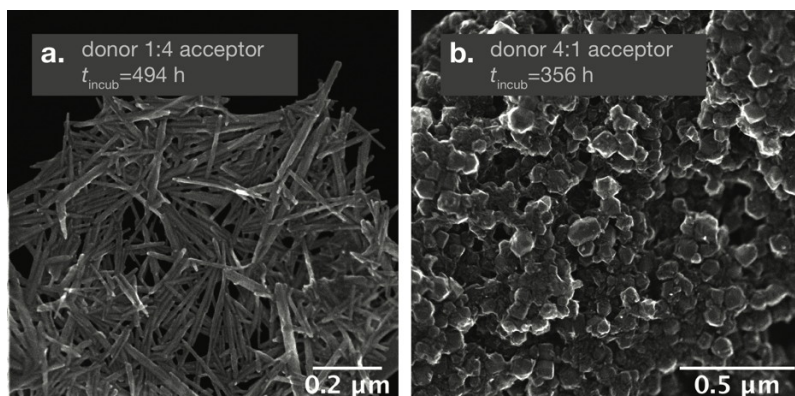
Figure S17 Selected electron microscopy images of iron oxides collected during incubations buffered to pH 7.0 using MOPS at initial donor-to-acceptor ratios of 1:4 (panel **a.**) and 4:1 (panel **b.**). The times of iron oxide suspension collection, t_{incub}, are reported on the plots. Images were recorded using a secondary electron detector.
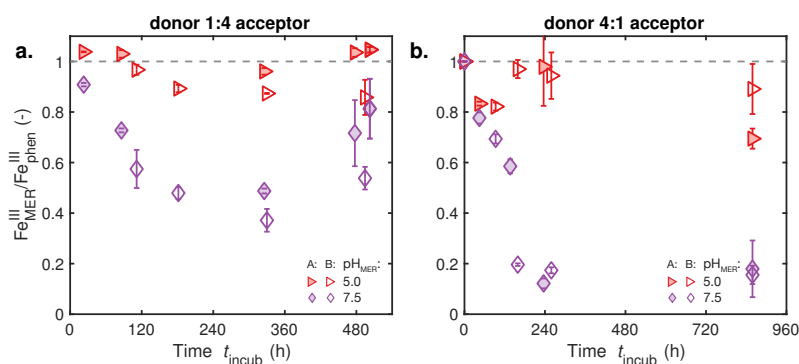

Figure S18 Changes in iron oxide reducibility during microbial iron oxide reduction as assessed using mediated electrochemical reduction (MER). Incubations were performed at initial donor-to-acceptor ratios of 1:4 (panel **a.**) and 4:1 (panel **b.**), both buffered to pH 7.0 using MOPS. MER data are shown for duplicate incubation vials (A and B in filled and open symbols, respectively). Changes in the extents of oxide-Fe^{III} reduction over the course of the incubations are shown. Reduction extents are presented as the fraction of total oxide-Fe^{III} reducible in MER ($Fe^{III}_{MER}/Fe^{III}_{phen}$). Fe^{III}_{phen} was determined using the phenanthroline assay (phen). MER measurements were performed at pH_{MER}=5.0 (red triangles) and 7.5 (purple diamonds), both at applied reduction potentials of $E_H^{MER} = -0.35$ V.

S11 Ferrous iron production and mineralogical transformation across all initial donor-to-acceptor ratios
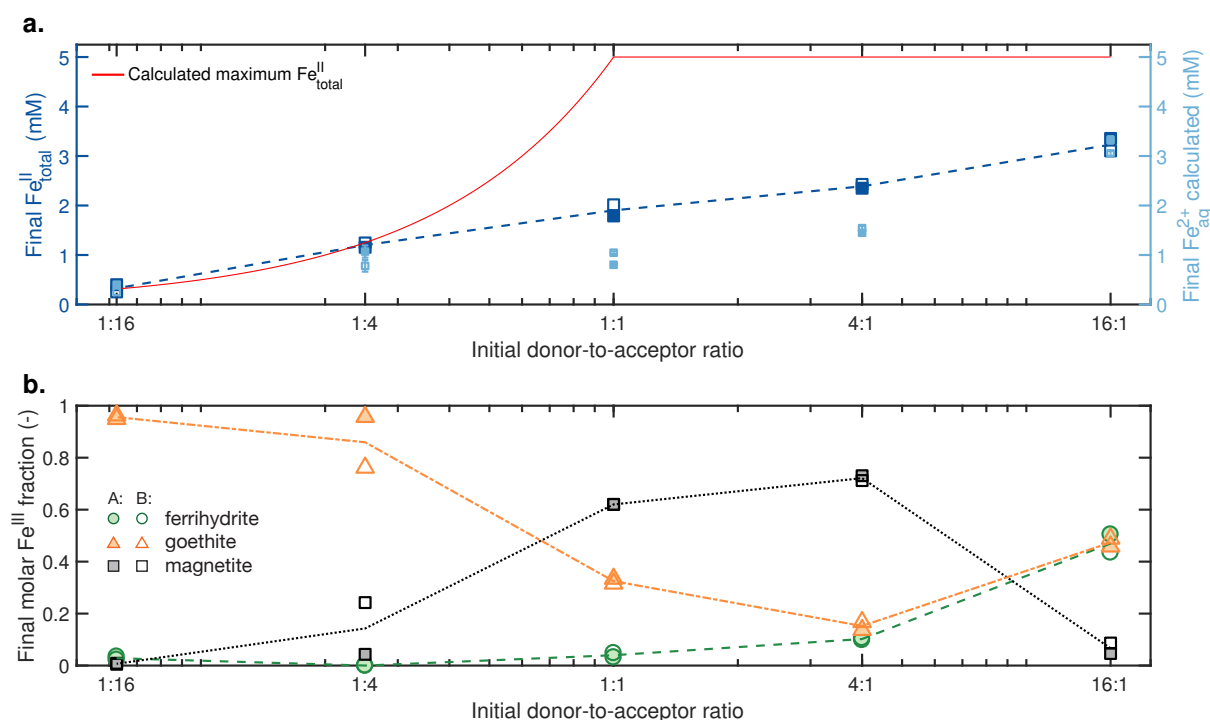

Figure S19 Concentrations of ferrous iron and iron oxide mineralogy at the end point of all incubations buffered to pH 7.0 using MOPS as a function of the initial donor-to-acceptor ratio. Data are shown for duplicate incubation vials (A and B in filled and open symbols, respectively). **a.** Concentrations of total Fe^{II} (final Fe^{II}_{total}, left y axis) and calculated aqueous Fe^{2+} (final Fe^{2+}_{aq}, right y axis) at the endpoints of the transformation experiments as a function of the initial donor-to-acceptor ratio. Fe^{II}_{total} was determined using the phenanthroline assay. Fe^{2+}_{aq} equals the difference between Fe^{II}_{total} and structural Fe^{II} in magnetite (calculated based on the concentration of Fe^{III} in magnetite and magnetite stoichiometry (Section S13)). The red line represents the maximum possible release of Fe^{II}_{total} based on the assumption that all added lactate was oxidized to acetate and the reducing equivalents liberated in this oxidation were transferred to oxide-Fe^{III}. **b.** Molar Fe^{III} fractions in ferrihydrite, goethite and magnetite at the endpoint of the transformation experiments as a function of the initial donor-to-acceptor ratio. Molar Fe^{III} fractions were determined by X-ray diffraction analysis.

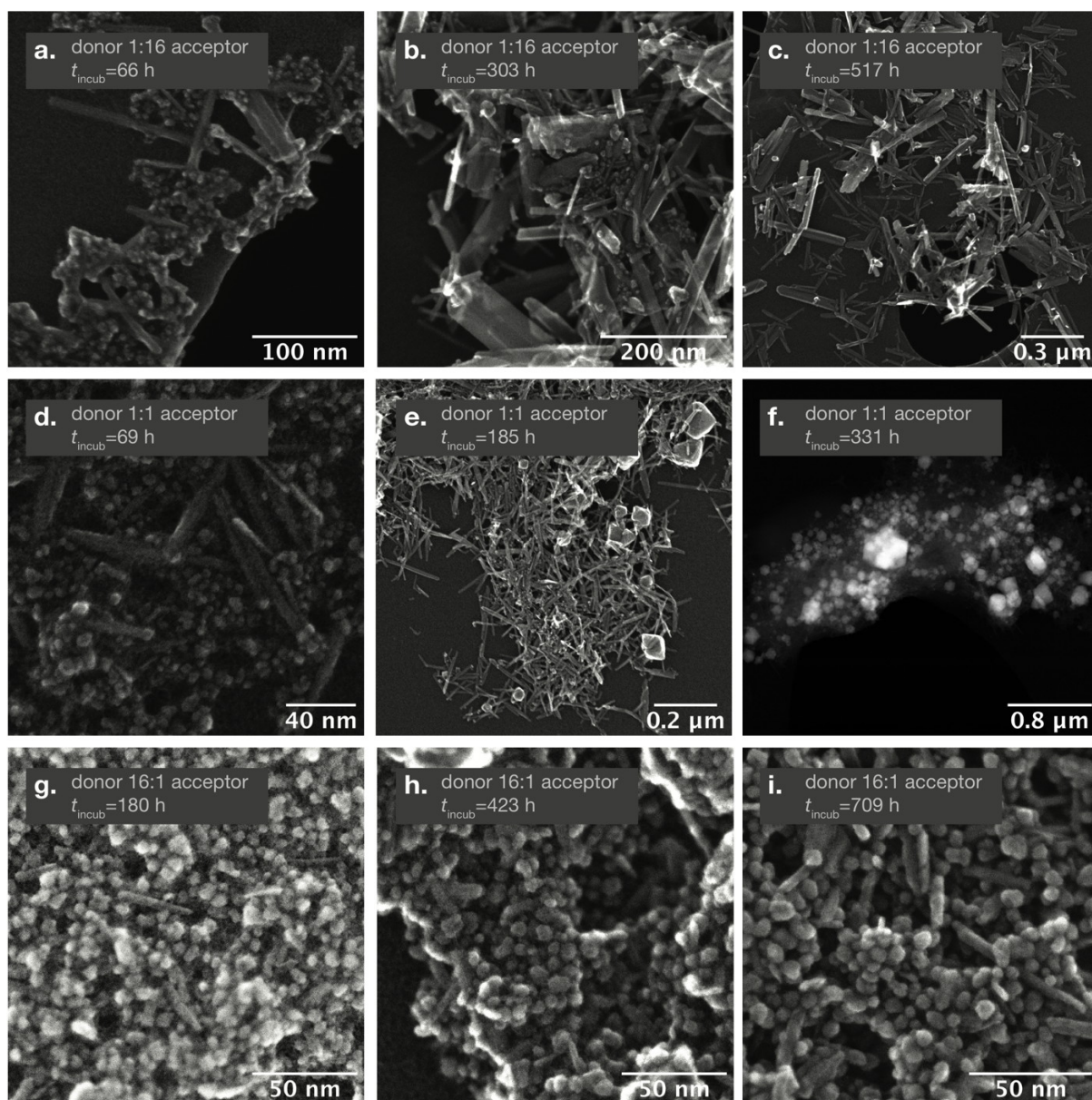# S12 Electron microscopy images

Figure S20 Selected electron microscopy images of iron oxides collected during incubations buffered to pH 7.0 using MOPS at initial donor-to-acceptor ratios of 1:16 (panels **a.-c.**), 1:1 (panels **d.-f.**) and 16:1 (panels **g.-i.**). The times of iron oxide suspension collection, t_{incub}, during the respective experiment are reported on the plots. Images were recorded using a high angular annular dark field detector (panel f.) or a secondary electron detector (remaining panels).

S13   Magnetite stoichiometry

Magnetite stoichiometry was determined from the fitted unit-cell length of magnetite according to the following eq. S1 (published in Figure 7 in Gorski and Scherer [8]).

$$x_d = \frac{a - 8.3424}{0.1094} \tag{S1}$$

where x_d is the stoichiometry of magnetite (i.e. the ratio of Fe^{II}/Fe^{III} in the magnetite structure), and a [Å] is the unit-cell length of magnetite derived from Rietveld fitting of X-ray diffractograms (Section S6).
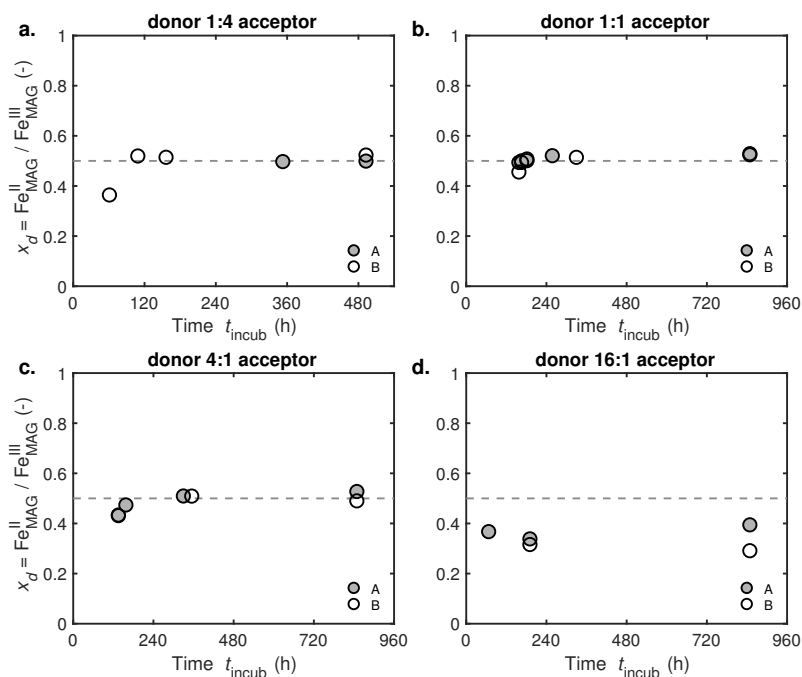

Figure S21 Changes in magnetite stoichiometry, $x_d = Fe^{II}_{MAG}/Fe^{III}_{MAG}$, during incubations buffered to pH 7.0 using MOPS at initial donor-to-acceptor ratios of 1:4 (panel **a.**), 1:1 (panel **b.**), 4:1 (panel **c.**) and 16:1 (panel **d.**). Note that no magnetite formed in the experiment at initial donor-to-acceptor ratio of 1:16. Data are shown for duplicate incubation vials (A and B in filled and open symbols, respectively). Magnetite stoichiometries were determined using eq. S1.

S14 Selected current responses in MER

a. donor 1:16 acceptor
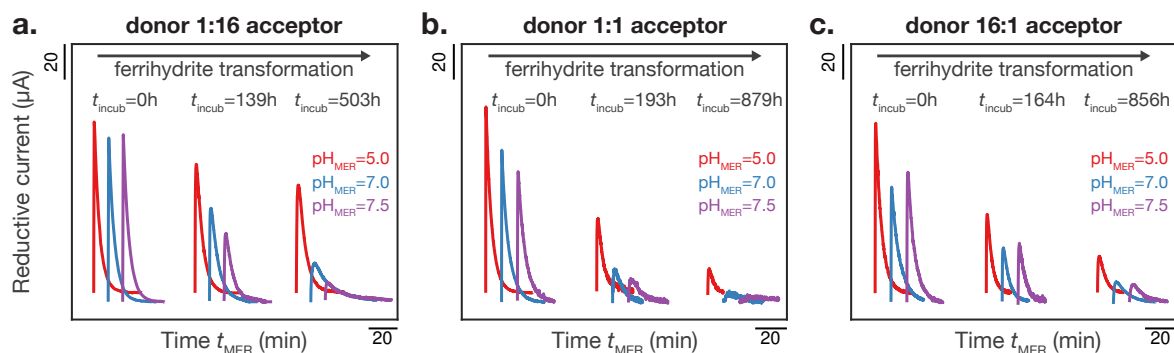**b.** donor 1:1 acceptor
c. donor 16:1 acceptor

Figure S22 Selected reductive current responses obtained during MER of iron oxide suspensions collected at the beginning, an intermediate time and the end of incubations buffered to pH 7.0 using MOPS at initial electron donor-to-acceptor ratios of 1:16 (panel **a.**), 1:1 (panel **b.**), and 16:1 (panel **c.**). The x axis label t_{MER} refers to the time (min) during MER measurements. The horizontal scale bar next to the axis label depicts a time span of 20 min. Current responses were obtained in MER at pH_{MER}=5.0 (red traces, replotted from Figure 2a-c), 7.0 (blue traces), and 7.5 (purple traces, replotted from Figure 3a-c), all at applied reduction potentials of $E_H^{MER} = -0.35$ V.
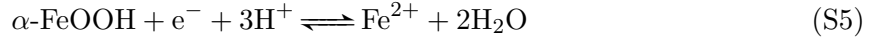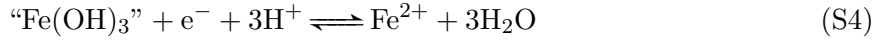
S15 Thermodynamic calculations

We calculated the reaction driving force for reductive iron oxide dissolution in MER, $\Delta_r G$ (J), using eq. S2.

$$\Delta_r G = -n \cdot F \cdot (E_H^{\text{oxide}} - E_H^{\text{MER}}) \tag{S2}$$

where n (mol) is the number of transferred electrons per overall reaction, F (C mol^{-1}) is the Faraday constant, E_H^{oxide} (V) is the reduction potential of the iron oxide, and E_H^{MER} (V) is the potential applied to the working electrode of the MER cell. We determined $\Delta_r G$ using $n=1$, i.e. for the transfer of one electron to one oxide-Fe$^{\text{III}}$. E_H^{oxide} was calculated using the Nernst equation S3.

$$E_H^{\text{oxide}} = E_H^0 - \frac{R \cdot T}{n_{e^-} \cdot F} \cdot 2.303 \cdot \left(m_{\text{Fe}_{\text{aq}}^{2+}} \cdot \log\left(\{\text{Fe}_{\text{aq}}^{2+}\}\right) + m_{\text{H}^+} \cdot \text{pH}_{\text{MER}} \right) \tag{S3}$$

where E_H^0 (V) is the standard reduction potential of the iron oxide ($E_H^0 = 0.98$ V for ferrihydrite[9] and $E_H^0 = 0.768$ V for goethite[10]), R is the gas constant, T ($= 298.15$ K) is the absolute temperature at which MER experiments were conducted, $\{\text{Fe}_{\text{aq}}^{2+}\}$ is the activity of aqueous Fe^{2+} (equals the product of the activity coefficient and the Fe$_{\text{aq}}^{2+}$ concentration), pH_{MER} is the pH of the solution in the MER cell, and n_{e^-}, $m_{\text{Fe}^{2+}}$, and m_{H^+} denote the stoichiometric coefficients for e$^-$, Fe^{2+}, and H$^+$ in the reductive dissolution equations for ferrihydrite (denoted for simplicity as "Fe(OH)$_3$") in eq. S4 or goethite (α-FeOOH) in eq. S5.

$$\text{"Fe(OH)}_3\text{"} + e^- + 3H^+ \rightleftharpoons Fe^{2+} + 3H_2O \tag{S4}$$

$$\alpha\text{-FeOOH} + e^- + 3H^+ \rightleftharpoons Fe^{2+} + 2H_2O \tag{S5}$$

We determined $\{\text{Fe}_{\text{aq}}^{2+}\}$ using an activity coefficient of 0.9 (calculated using the Davies equation and an ionic strength of 0.01 M in the MER cell) and a Fe$_{\text{aq}}^{2+}$ concentration of $4.55\cdot10^{-05}$ M (i.e., the concentration in the MER cell at the end of the measurement when Fe$^{\text{III}}$ is completely reduced)[11].

References

[1] Schwertmann, U., and Cornell, R. M. *Iron Oxides in the Laboratory: Preparation and Characterization*; Wiley-VCH, 2000.

[2] Myers, C. R., and Nealson, K. H. (1988) Bacterial manganese reduction and growth with manganese oxide as the sole electron acceptor. *Science 240*, 1319–1321.

[3] Zachara, J. M., Kukkadapu, R. K., Fredrickson, J. K., Gorby, Y. A., and Smith, S. C. (2002) Biomineralization of poorly crystalline Fe(III) oxides by dissimilatory metal reducing bacteria (DMRB). *Geomicrobiol. J. 19*, 179–207.

[4] Fredrickson, J. K., Zachara, J. M., Kennedy, D. W., Dong, H., Onstott, T. C., Hinman, N. W., and Li, S.-m. (1998) Biogenic iron mineralization accompanying the dissimilatory reduction of hydrous ferric oxide by a groundwater bacterium. *Geochim. Cosmochim. Acta 62*, 3239–3257.

[5] Aeppli, M., Kaegi, R., Kretzschmar, R., Voegelin, A., Hofstetter, T. B., and Sander, M. (2019) Electrochemical Analysis of Changes in Iron Oxide Reducibility during Abiotic Ferrihydrite Transformation into Goethite and Magnetite. *Environ. Sci. Technol. 53*, 3568–3578.

[6] Scarlett, N. V. Y., and Madsen, I. C. (2006) Quantification of phases with partial or no known crystal structures. *Powder Diffr. 21*, 278–284.

[7] ThomasArrigo, L. K., Byrne, J. M., Kappler, A., and Kretzschmar, R. (2018) Impact of organic matter on iron(II)-catalyzed mineral transformations in ferrihydrite–organic matter coprecipitates. *Environ. Sci. Technol. 52*, 12316–12326.

[8] Gorski, C. A., and Scherer, M. M. (2010) Determination of nanoparticulate magnetite stoichiometry by Mössbauer spectroscopy, acidic dissolution, and powder X-ray diffraction: A critical review. *Am. Mineral. 95*, 1017–1026.

[9] Fischer, W. R. (1987) Standard potentials (E$_0$) of iron(III) oxides under reducing conditions. *Z. Pflanzenernähr. Bodenkd. 150*, 286–289.

[10] Gorski, C. A., Edwards, R., Sander, M., Hofstetter, T. B., and Stewart, S. M. (2016) Thermodynamic characterization of iron oxide-aqueous Fe^{2+} redox couples. *Environ. Sci. Technol. 50*, 8538–8547.

[11] Aeppli, M., Voegelin, A., Gorski, C. A., Hofstetter, T. B., and Sander, M. (2018) Mediated electrochemical reduction of iron (oxyhydr-)oxides under defined thermodynamic boundary conditions. *Environ. Sci. Technol. 52*, 560–570.